Lithuanian Journal of Physics, Vol. **44**, No. 4, pp. 267–273 (2004)

HOLE SPIN SURFACES IN A_3B_5 SEMICONDUCTORS

A. Dargys

Semiconductor Physics Institute, A. Goštauto 11, LT-01108 Vilnius, Lithuania
E-mail: dargys@pfi.lt

Received 12 February 2004

The Hamiltonian of A_3B_5 semiconductors apart from quadratic in wave vector $\mathbf{k}$ terms also contains linear terms. The latter originate from the spin–orbit interaction in semiconductors without inversion symmetry. The paper investigates hole spin properties of A_3B_5 semiconductors – GaAs, InAs, GaP, InP, GaSb, and InSb – paying special attention to contribution of the linear-$\mathbf{k}$ terms. It is shown that the general properties of the hole spin surfaces in the mentioned compounds are similar to those in elementary semiconductors investigated recently. It has been found that the influence of linear-$\mathbf{k}$ terms on band spins is weak and, as a result, the deformation of the spin surfaces is insignificant.

Keywords: semiconductors, spintronics, valence band, spin control

PACS: 71.70.Ms, 72.20.Jv, 73.40.Gk, 78.55.–m, 79.90.+b

1. Introduction

In the last decade, in the rapidly developing area of the spintronics, especially in the 2D semiconductor and metal spintronics, the main attention was focused on the properties of the electron rather than hole spin properties. The current status of the spintronics is fully reflected in the Proceedings of the PASPS Conference [1]. The main advantage of the electron spintronics against valence-band hole spintronics is long lifetime of electron spin in the elementary and compound semiconductors: hundreds or more collisions with phonons and impurity atoms are needed for an electron to loose its spin memory. In contrast, due to strong spin–orbit interaction in the valence bands of elementary, A_3B_5 and other compound semiconductors, the hole spin is lost after a few collisions with the lattice phonons. However, in the ultrafast and coherent spintronics, where spin-switching times are shorter than the carrier momentum scattering time, this drawback may not be detrimental in the operation of the ultrafast spintronic devices. Recently, by solving the time-dependent Schrödinger equation for coupled valence bands, it was shown that the intervalence tunnelling of holes in high electric fields can induce flipping of the hole spin [2–4]. Such flipping can be achieved if optimized π-type electric pulses (such pulses transfer the hole from one to the other band with the probability equal one) are applied.

In the case of the electrons the spin dynamics, due to the simplicity of the conduction band, usually takes place on a single spherically-shaped spin surface. However, in the case of holes, as shown recently in [2–4], the spin flipping or switching occurs between different spin surfaces that describe different (heavy-mass, light-mass or split-off) bands. In papers [3, 4] it was also shown that in p-type silicon the spin switching time may be shorter than a picosecond for heavy–light band transitions and a hundred of femtoseconds for heavy–split-off band transitions. Since in the spin-flipping dynamics in valence bands the transitions between different spin surfaces predominate, in the optimization of spin switching times one should pay special attention to the form of the initial and final spin surfaces coupled by controlling field during switching.

As mentioned, in the conduction bands the electron spin surfaces both in the elementary and compound semiconductors are spherically shaped or very close to a sphere. However, for valence bands, due to strong spin–orbit interaction, the spin surfaces may substantially deviate from the sphere as shown recently in [5, 6]. In an extreme case the spin surface may shrink to a line, for example, when the heavy-mass hole propagates in high-symmetry direction, especially in $[001]$-type directions. Here the reader should be reminded that the terms "electron spin" and "hole spin," as it is common in the spintronics, are not strict enough. In fact it would be better to use the term "total an-

ISSN 1648-8504

gular momentum." In the case of conduction band electrons of elementary and A_3B_5 semiconductors this makes no difference, since the orbital quantum number of the conduction band is $L = 0$. However, for valence bands one has $L = 1$, and the total angular momentum, $J = L + S$, is different from S. In this paper we shall be interested in the properties of J. The pure spin S in p-type semiconductors may be important, for example, in the exchange interaction of a free hole with a magnetic centre, say, in GaAs heavily doped with Mn impurities, where due to the proximity of the hole and Mn atom, the pure spin S rather than orbital motion determines the strength of the magnetic interaction [7]. In this paper, weakly doped semiconductors will be considered, where the ballistic hole injected into one of the valence bands is characterized by some wave vector $\mathbf{k}$. In this case J rather than S determines the magnetic properties of the hole.

In papers [5, 6], spin properties of the tetrahedral semiconductors such as p-type silicon or germanium, the elementary cell of which possesses the inversion symmetry, was considered. In such semiconductors all bands are doubly degenerate all over the Brillouin zone. In this paper the spin properties of holes in A_3B_5 compounds, the elementary cell of which is not invariant with respect to inversion, are presented. The absence of the inversion gives rise to linear-$\mathbf{k}$ terms in the valence band Hamiltonian, what results in the removal of double degeneracy of the valence bands, or the appearance of the so-called spin splitting. The spin splitting may be important in the behaviour of the freely propagating hole spin. The purpose of this paper is to investigate to what extent the shape of hole spin surfaces is influenced by inclusion of the linear-$\mathbf{k}$ terms in the Hamiltonian of A_3B_5 compounds. As known, in optics such linear-$\mathbf{k}$ terms give rise to electrooptic Pockels effect.

2. Linear-k terms

As mentioned, the lack of the inversion symmetry in A_3B_5 semiconductors brings about linear-$\mathbf{k}$ terms in the valence band Hamiltonian. Linear-$\mathbf{k}$ mixing within Γ_8 valence states (heavy- and light-mass bands) was considered by Kane [8, 9] and its contribution was evaluated by $\mathbf{k}\cdot\mathbf{p}$ and LMTO (linear muffin-tin orbitals) methods by Cardona et al. [10, 11]. The linear-$\mathbf{k}$ Hamiltonian for both Γ_8 and Γ_7 (split-off) valence bands in bulk semiconductors and heterostructures was recently evaluated by Foreman [12], who demonstrated that its contribution in heterostructures is by an order

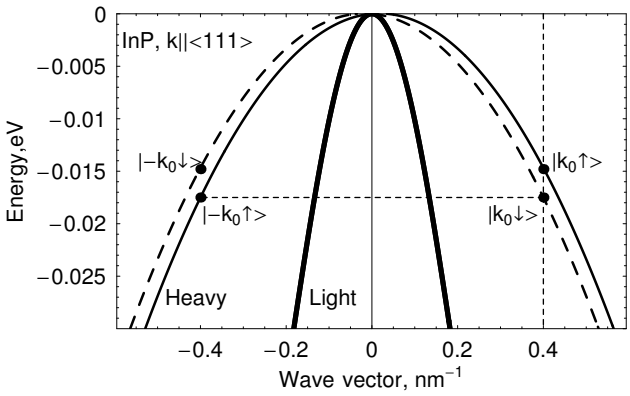

Fig. 1. Heavy- and light-mass hole dispersion curves for InP when $\mathbf{k}\|\langle 111\rangle$. In this direction the spin splitting occurs in the heavy-mass band only. The dashed vertical line shows that a ballistic hole with the wave vector $\mathbf{k}_0$ may have an uncompensated spin in the mixed state. The horizontal line shows how compensation of the hole spin occurs at thermal equilibrium.

larger than in the bulk semiconductors. Rewritten in the Luttinger–Kohn [13] basis $|J, m\rangle$, where J is the total angular momentum and m represents its projections, the linear-$\mathbf{k}$ part of the Hamiltonian in the atomic units ($e = \hbar = m_0 = 1$) reads [12]

$$\widehat{H}_1 = \begin{bmatrix} 0 & -\mathrm{i}\kappa & -\lambda & \mathrm{i}\sqrt{3}\kappa^\dagger & \mu & -\mathrm{i}\nu \\ \mathrm{i}\kappa^\dagger & 0 & \mathrm{i}\sqrt{3}\kappa & \lambda & 0 & \sqrt{3}\mu \\ -\lambda & -\mathrm{i}\sqrt{3}\kappa^\dagger & 0 & -\mathrm{i}\kappa & -\sqrt{3}\mu^\dagger & 0 \\ -\mathrm{i}\sqrt{3}\kappa & \lambda & \mathrm{i}\kappa^\dagger & 0 & \mathrm{i}\nu & -\mu^\dagger \\ \mu^\dagger & 0 & -\sqrt{3}\mu & -\mathrm{i}\nu & 0 & 0 \\ \mathrm{i}\nu & \sqrt{3}\mu^\dagger & 0 & -\mu & 0 & 0 \end{bmatrix}. \tag{1}$$

The basis function $|J, m\rangle$ ordering in the matrix (1) is $|\frac{3}{2}, \frac{3}{2}\rangle$, $|\frac{3}{2}, \frac{1}{2}\rangle$, $|\frac{3}{2}, -\frac{1}{2}\rangle$, $|\frac{3}{2}, -\frac{3}{2}\rangle$, $|\frac{1}{2}, \frac{1}{2}\rangle$, $|\frac{1}{2}, -\frac{1}{2}\rangle$. In Eq. (1),

$$\kappa = \frac{1}{2}c(k_x + \mathrm{i}k_y),$$

$$\lambda = ck_z,$$

$$\mu = \frac{1}{2\sqrt{2}}c'(k_x + \mathrm{i}k_y),$$

$$\nu = \frac{1}{\sqrt{2}}c'k_z.$$

The wave vector $\mathbf{k} = (k_x, k_y, k_z)$ is reference to crystallographic axes. The empirical coefficient c couples Γ_8 state manifold, while the coefficient c' couples Γ_7 states to Γ_8 states.

Table 1. Valence band parameters γ_1, γ_2, γ_3, and Δ, $\mathbf{k}$-linear coefficient c, spin splitting energy $\Delta\varepsilon_{ss}$, and the maximum wave vector $k^{\max}_{\langle 111\rangle} = \pi/a$ at L point of the Brillouin zone of A_3B_5 semiconductors. Valence band parameters and lattice constant a were taken from [15]. The coefficient c was taken from [11]. $\Delta\varepsilon_{ss}$ corresponds to hole wave vector $\mathbf{k} = 0.283(1,1,1)$ nm^{-1}.

Semiconductor	γ_1	γ_2	γ_3	Δ eV	c meV·Å	$\Delta\varepsilon_{ss}$ meV	$k^{\max}_{\langle 111\rangle}$ nm^{-1}
GaAs	6.98	2.06	2.93	0.341	−3.4	0.47	5.56
InAs	20.0	8.5	9.2	0.39	−11.2	1.57	5.19
GaP	4.05	0.49	1.25	0.08	−5.5	0.76	5.76
InP	5.08	1.6	2.10	0.108	−14.4	2	5.35
GaSb	13.4	4.7	6.0	0.76	+0.7	0.1	5.15
InSb	34.8	15.5	16.5	0.81	−8.2	1.13	4.85

The total six-band valence Hamiltonian consists of two terms:

$$\widehat{H} = \widehat{H}_0 + \widehat{H}_1. \tag{2}$$

The first one $\widehat{H}_0$ is the well-known matrix which is made up of the elements quadratic in the wave vector elements [13, 14]. It is characterized by three empirical parameters γ_1, γ_2, γ_3, and by the strength Δ of spin–orbit splitting between Γ_8 and Γ_7 bands at the point $\mathbf{k} = 0$. $\widehat{H}_0$ is the main contribution in the elementary semiconductor valence-band Hamiltonian that represents the doubly degenerate heavy-mass (h), light-mass (l), and split-off (s) energy bands as well as the spin properties in these semiconductors [6]. In general, the total Hamiltonian (2) with the linear-$\mathbf{k}$ part H_1 included yields nonparabolic, nonspherical, and nondegenerate (except at some high symmetry points) energy bands. As an illustration, in Fig. 1 heavy- and light-mass bands in InP along $\langle 111\rangle$ direction are plotted, with the linear-$\mathbf{k}$ terms included. γ_1, γ_2, γ_3, and Δ values were taken from the recent review [15] on A_3B_5 semiconductors and their alloys. The parameter c was taken from [11, 12] (see also Table 1). To author's knowledge the magnitude of the parameter c' is not known as yet. In calculations it was assumed that $c' = 0.05c$. Figure 1 shows that for $\mathbf{k}\|\langle 111\rangle$ only the heavy-mass band suffers spin splitting. The light-mass band remains doubly degenerate. This is in agreement with the group-theoretical calculations in [16], from which follows that in T_d symmetry crystals the light-mass band does not split at the points that lie on the third-order axes. In general, symmetry considerations show that the spin splitting due to linear-$\mathbf{k}$ terms may occur in all Brillouin zone points where $\mathbf{k} \neq 0$, except the points which lie on the fourth-order axes, e. g., on $[100]$-type or equivalent axes. Thus, all bands will be spin split if, for example, $\mathbf{k}$ is pointing in $[110]$ direction.

In Table 1, the column next to the last shows the magnitude of the spin splitting $\Delta\varepsilon_{ss}$ in the heavy-mass band at the wave vector $\mathbf{k} = (k_x, k_y, k_z) = 0.283(1,1,1)$ nm^{-1}, which is about 5% off the centre of the Brillouin zone. From this table it follows that the spin splitting in the commonly used A_3B_5 semiconductors is of the order of 1 meV. This justifies the neglect of the spin splitting of the bands in the calculation of hole transport properties [17].

Figure 1 also explains the meaning of Kramers degeneracy that is related with valence band spin. The Kramers degeneracy [18] requires a state $|\mathbf{k}\downarrow\rangle$, where the arrow indicates the down spin, to have the same energy as another state $|-\mathbf{k}\uparrow\rangle$ in solids. Thus, at $\mathbf{k} = \mathbf{k}_0$ only the states with energies $\varepsilon(\mathbf{k}_0\downarrow) = \varepsilon(-\mathbf{k}_0\uparrow)$ on the horizontal line shown in Fig. 1 are degenerate due to time reversal. This is, partly, because the time reversal symmetry duplicates some of the important features of the inversion symmetry. As a result, in thermal equilibrium the total magnetization of p-type semiconductor is zero. However, the Kramers degeneracy is absent if one considers the ballistic hole that propagates in the spintronic device and has a well-defined wave vector $\mathbf{k}_0$ (the vertical line in Fig. 1). Such hole can be in one of the pure states, $|\mathbf{k}_0\uparrow\rangle$ or $|\mathbf{k}_0\downarrow\rangle$ that are characterized by different eigenenergies, or in a mixture of these states. Normally, the spin splitting energy $\Delta\varepsilon_{ss} = \varepsilon(\mathbf{k}_0\uparrow) - \varepsilon(\mathbf{k}_0\downarrow)$ is much smaller than the hole thermal energy kT, therefore, the hole will be in a mixture of the mentioned pure states, i. e. its energy will be slightly smeared. The degree of the smearing, or mixing of the states $|\mathbf{k}_0\uparrow\rangle$ and $|\mathbf{k}_0\downarrow\rangle$, as we shall see in the next section, is closely related with the hole spin surfaces. It will be shown that the spin splitting in A_3B_5 compounds plays much greater role in spintronics as compared to hole transport properties.

3. Spin surfaces in A_3B_5 compounds

The shapes of hole spin surfaces for the wave vectors having various symmetry when spin splitting is absent was considered in detail in [6]. Here only the main steps which are needed to understand the results with the spin splitting included are described.

Since the matrices $\widehat{H}$ and $\widehat{\mathbf{J}}$ do not commute, in calculating the average value of the hole spin $\langle \mathbf{J} \rangle$ one, at first, should select a concrete representation, either energy or total angular momentum representation. The latter representation has been used in the construction of the linear part of the Hamiltonian (2) [12]. In the semiconductor physics in the analysis of the transport properties in high electric fields it is common to assume that the charge carrier state is characterized by a particular energy in the energy band. For this reason the hole wave functions in the energy representation will be used as a starting point in this paper. In the numerical calculations the following parametrization of the six-component heavy- and light-mass band spinors in the energy representation was employed:

$$f_h = \left(a_h, \mathrm{e}^{\mathrm{i}\phi_h}\sqrt{1-a_h^2}, 0, 0, 0, 0\right), \tag{3}$$

$$f_l = \left(0, 0, a_l, \mathrm{e}^{\mathrm{i}\phi_l}\sqrt{1-a_l^2}, 0, 0\right). \tag{4}$$

The following order of bands is assumed:

$$\left(f_h^{(\uparrow)}, f_h^{(\downarrow)}, f_l^{(\uparrow)}, f_l^{(\downarrow)}, f_s^{(\uparrow)}, f_s^{(\downarrow)}\right),$$

where the subscript denotes heavy-, light-mass or split-off bands and the superscript describes the spin state. The spinors (3) and (4) are normalized to unity. The average spin projections on the crystallographic axes were calculated from

$$\langle J_j \rangle_i = \langle \psi_i | J_j | \psi_i \rangle, \tag{5}$$

where $|\psi\rangle$ is the spinor in the total angular momentum (or Luttinger–Kohn) representation $|J, m\rangle$ and J_j is jth Cartesian projection of the total 6×6 angular momentum matrix. The subscript j denotes the Cartesian component (x, y or z) and the subscript i denotes the band ($i = h$, l or s). The concrete forms of the matrices J_j can be found in [6]. $|\psi\rangle$ is related to $|f\rangle$ by unitary transformation: $|\psi\rangle = \widehat{T}|f\rangle$, where the transformation matrix $\widehat{T}$ relates the Hamiltonian (2) in the total angular momentum representation with its energy-diagonal counterpart in the energy representation: $\widehat{H}_\mathrm{d} = \widehat{T}^\dagger \widehat{H} \widehat{T}$. The numerical singular value decomposition [19, 20] was used to find the matrix $\widehat{T}$.

Figures 2 and 3 show the spin surfaces of the light-mass hole for InP and GaP, respectively. The figures

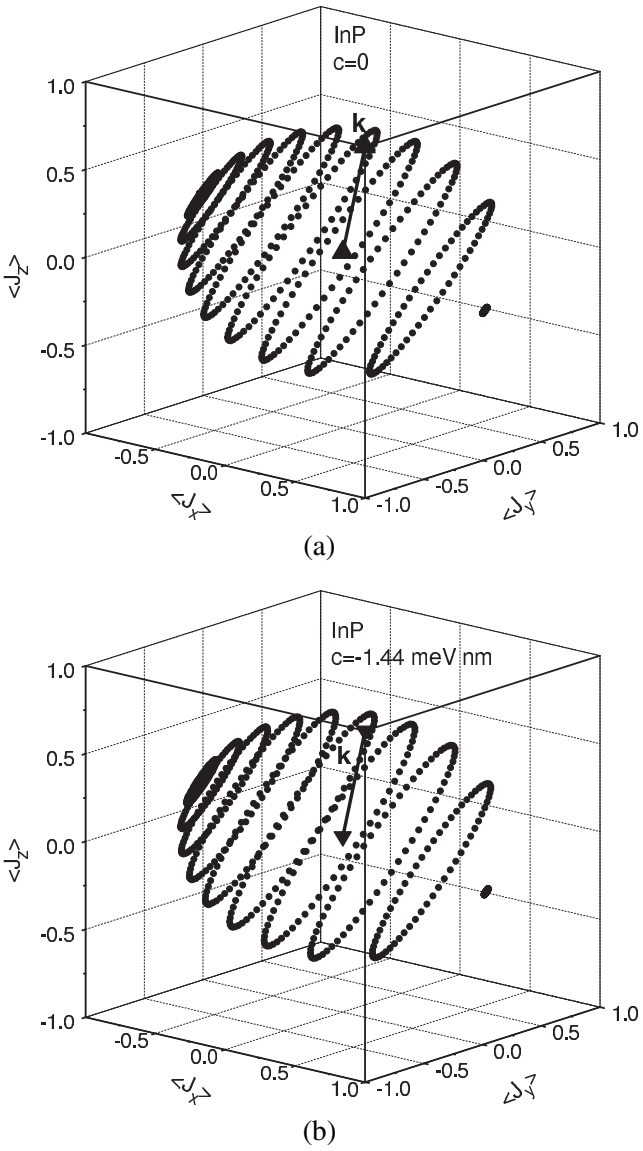

Fig. 2. Light-mass spin surfaces for InP (a) in the absence, $c = 0$, and (b) in the presence, $c = -14.4$ meV·Å, of the spin splitting. $\mathbf{k} = 0.283(1, -1, 1)$ nm^{-1}. The direction of the wave vector is drawn between the two triangle-shaped points.

are typical of other A_3B_5 compounds, too. The surfaces are represented by points at equally spaced values of a_l and ϕ_l in Eq. (4) in the range $a_l = 0{-}1$ and $\phi_l = 0{-}2\pi$, and steps $\Delta a_l = 0.1$, $\Delta\phi_l = 0.1$ or smaller. Figure 2 represents the spin surface in three dimensions and Fig. 3 represents its projection on the $\langle J_x \rangle - \langle J_y \rangle$ plane. Panels (a) in Figs. 2 and 3 show the surfaces when the spin splitting is absent ($c = c' = 0$) and panels (b) show the effect of inclusion of linear-$\mathbf{k}$ Hamiltonian $\widehat{H}_1$ in the total Hamiltonian (2). The pure states have $a_l = 0$ and $a_l = 1$ which represent two opposite poles on the spin surfaces. From Figs. 2 and 3 it can be concluded that the contribution of the linear-$\mathbf{k}$

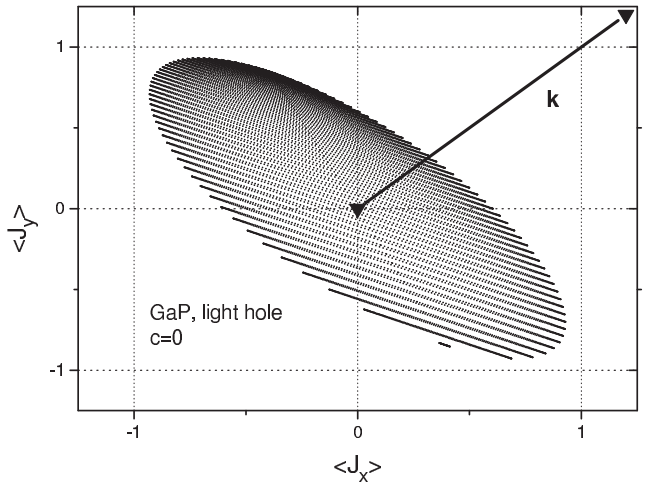

(a)

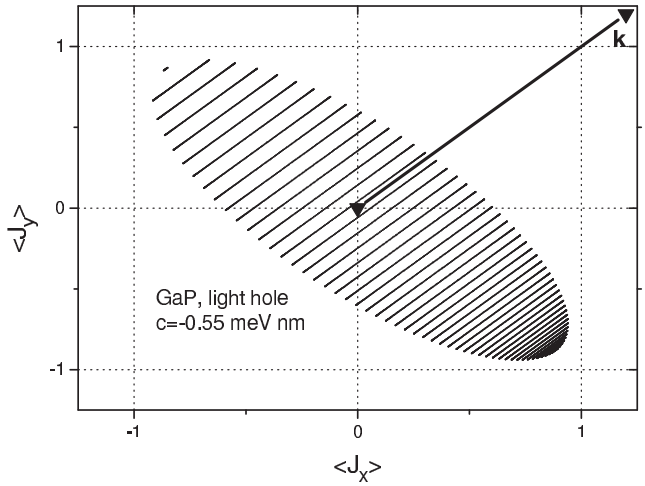

(b)

Fig. 3. Projection of the light-mass spin surface on $\langle J_x\rangle - \langle J_y\rangle$ plane for GaP (a) in the absence, $c = 0$, and (b) in the presence, $c = -5.5$ meV·Å, of the spin splitting. $\mathbf{k} = 0.019(1, 1, 0)$ nm^{-1}.

term is very small in InP as well as GaP. Calculations with parameters of other semiconductors in Table 1 gave similar or intermediate graphs to those shown in Figs. 2 and 3.

Figure 4 shows heavy-mass spin surface in InSb calculated with spinor (3). Now the surface is needle-like, the points of which are very close to $[1\bar{1}1]$ line. In the plot of the Fig. 4 the cases $c = 0$ and $c = -8.2$ meV·Å are practically indistinguishable. In the limit $\mathbf{k} \to 0$, the points lie exactly on the $[1\bar{1}1]$ line. Similar calculations with the parameters of Table 1 gave nearly identical results to those shown in Fig. 4 – in all cases the points were found to lie very close to $[1\bar{1}1]$ line. As shown in [6], for all equivalent directions of $\mathbf{k}$ one can find equivalent spin surfaces. Thus, in analogy to the wave vector star which reflects the presence of symmetry operation between equivalent $\mathbf{k}$'s, one can construct a manifold of the equivalent spin surfaces, or the star of the spin surfaces.

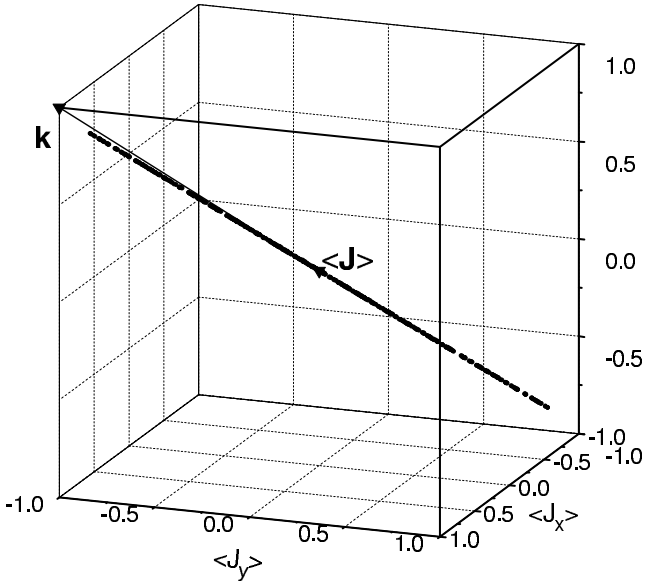

Fig. 4. Heavy-mass spin surface $\langle\mathbf{J}\rangle$ for InSb, when $c = -8.2$ meV·Å. The surface has a needle-like shape and is nearly parallel to $\mathbf{k}\|[1\bar{1}1]$. If $c = 0$, then $\langle\mathbf{J}\rangle\|\mathbf{k}\|[1\bar{1}1]$.

To have a quantitative estimate of the contribution of linear-$\mathbf{k}$ terms in the deformation and rotation of the spin surface the results for various semiconductors are summarized in Table 2. For this purpose the average spin radius at $c = 0$ and $c \neq 0$ was introduced,

$$|\langle\mathbf{J}\rangle| = \sqrt{\langle J_x\rangle^2 + \langle J_y\rangle^2 + \langle J_z\rangle^2}, \tag{6}$$

as well as its minimum and maximum values, $|\langle\mathbf{J}\rangle|^{\min}$ and $|\langle\mathbf{J}\rangle|^{\max}$. These parameters describe an overall shape of the spin surfaces. The deviations from $|\langle\mathbf{J}\rangle|^{\min}$ and $|\langle\mathbf{J}\rangle|^{\max}$, when c and c' are included, were described by the quantity

$$\Delta|\langle\mathbf{J}\rangle| = |\langle\mathbf{J}\rangle|_{c\neq 0} - |\langle\mathbf{J}\rangle|_{c=0}. \tag{7}$$

In Table 2, $\Delta|\langle\mathbf{J}\rangle|^{\min}$ and $\Delta|\langle\mathbf{J}\rangle|^{\max}$ represent the minimum and maximum deviations (7) from the average values (6). The following points should be noted upon inspection of the Table 2.

Depending on the magnitude of a_h and ϕ_h in spinor (3), the absolute value of the heavy-mass hole spin $|\langle\mathbf{J}\rangle|_h$ may have any value in the range from $-3/2$ to $3/2$. For parabolic and spherical bands the spin $\langle\mathbf{J}\rangle_h$ is line which is parallel to hole wave vector $\mathbf{k}$ [6]. This property is preserved for all directions of $\mathbf{k}$, although, in real semiconductors the degeneracy of spin states is lifted and, as result, heavy hole

Table 2. The minimum $|\langle \mathbf{J} \rangle|^{\min}$ and maximum $|\langle \mathbf{J} \rangle|^{\max}$ angular momentum for degenerate bands of A_3B_5 semiconductors and the deviations, $\Delta|\langle \mathbf{J} \rangle|^{\min}$ and $\Delta|\langle \mathbf{J} \rangle|^{\max}$, from $|\langle \mathbf{J} \rangle|^{\min}$ and $|\langle \mathbf{J} \rangle|^{\max}$, respectively, when the spin splitting is taken into account. Here $\mathbf{k} = 0.019(1,1,0)$ nm^{-1}

Semiconductor	Band	$c = c' = 0$		$c \neq c' \neq 0$	
		$\lvert\langle \mathbf{J} \rangle\rvert^{min}$	$\lvert\langle \mathbf{J} \rangle\rvert^{\max}$	$\Delta\lvert\langle \mathbf{J} \rangle\rvert^{\min}$	$\Delta\lvert\langle \mathbf{J} \rangle\rvert^{\max}$
GaAs	light	0.49	1.11	∼0%	∼0%
	heavy	0.115	1.5	∼8%	∼0%
InAs	light	0.5	1.03	∼0%	∼1%
	heavy	0.03	1.5	∼0%	∼0%
GaP	light	0.455	1.23	∼0%	∼1%
	heavy	0.234	1.45	∼8%	∼0%
InP	light	0.494	1.09	∼0%	∼4%
	heavy	0.09	1.5	∼0%	∼0%
GaSb	light	0.495	1.08	∼0%	∼0%
	heavy	0.08	1.5	∼0%	∼0%
InSb	light	0.5	1.02	∼10%	∼0%
	heavy	0.02	1.5	∼0%	∼0%

spin surfaces become cigar-shaped ellipsoids. In Table 2 this is reflected in the finite value of $|\langle \mathbf{J} \rangle|^{\min}$. In $\langle 100 \rangle$ and $\langle 111 \rangle$ directions the minor axis of the heavy-mass ellipsoid is very small and, as Fig. 4 shows, the surface is similar to a line. However, in $\langle 110 \rangle$-type directions, the minor axis is larger, especially in GaP, where the ratio of minor to major axes reaches 0.14 (see Table 2). The inclusion of spin splitting has very little effect on the shape of the heavy-mass hole spin surface, although, as seen from Fig. 4, now the cigar is not exactly parallel to the wave vector.

As concerns the light-mass band, from Table 2 and from Figs. 2 and 3 it is seen that the spin surfaces are not spherical. In the limit of parabolic and spherical bands the light hole spin surfaces reduce to the oblate ellipsoid, the major and minor axes of which are $\langle \mathbf{J} \rangle_l^{\max} = 1$ and $\langle \mathbf{J} \rangle_l^{\min} = 1/2$, with the minor axis being parallel to $\mathbf{k}$. Table 2 shows that the largest deviations from these values are in GaP. The inclusion of the spin splitting, in general, has little effect on the shape of the spin surfaces in this case, too. It should be noted that in the valence band spectrum for small values of $\mathbf{k}$, by contrast, the linear-$\mathbf{k}$ terms are important. It should be remembered that in the present calculations the third, spin–orbit split-off band was included too, since, due to strong light–split-off band interaction, the light-mass band spin depends indirectly on valence band parameters, for example, on the split-off energy Δ, that determine the properties of the split-off band as well.

Apart from linear-$\mathbf{k}$ terms, the hole spin may also depend on higher-order, e. g., cubic-$\mathbf{k}$ terms, especially if the hole energy is large and the wave vector points in $[110]$-type direction [11]. In this direction all bands experience spin splitting. In this paper the analysis of the influence of higher-order terms in $\mathbf{k}$ was not undertaken, because of the uncertainty in the coefficient c' that describes lower, i. e. the first-order Hamiltonian (1) in the total Hamiltonian.

In conclusion, numerical analysis of spin surfaces of A_3B_5 semiconductors shows that the heavy and light hole spin surfaces deviate from those which follow from the simple spherical and parabolic band model. However, inclusion of the linear-$\mathbf{k}$ terms in the valence band Hamiltonian gives that their influence on the hole spin properties, in general, is small. Therefore, in the analysis of spin dynamics under ultrashort pulse excitation a simpler band model which neglects spin splitting and which is frequently used in the transport analysis can be addressed.

References

[1] *Proceedings of the PASPS Conference*, J. Superconductivity: Incorporating Novel Magnetism **16**(1, 2) (2003).

[2] A. Dargys and P. Harrison, Hole spin dynamics in constant and alternating electric fields, Semicond. Sci. Technol. **18**(4), 247–252 (2003).

[3] A. Dargys, Ultrafast control of hole spin by electric field in semiconductors, IEEE J. Selected Topics Quantum Electron. **10**(1), 155–158 (2004).

[4] A. Dargys, Control of valence-band hole spin by electric field, Acta Phys. Pol. **105**(3), 295–306 (2004).

[5] A. Dargys, Coherent properties of hole spin, Lithuanian J. Phys. **43**(2), 123–128 (2003).

[6] A. Dargys, Spin surfaces and trajectories in valence bands of tetrahedral semiconductors, Phys. Status Solidi B **241**(1), 145–154 (2004).
[7] M. Abolfath, T. Jungwirth, J. Brum, and A.H. MacDonald, Theory of magnetic anisotropy in $III_{1-x}Mn_xV$ ferromagnets, Phys. Rev. B **63**(5), 054418-1–14 (2001).
[8] E.O. Kane, in: *Semiconductors and Semimetals*, Vol. 1, eds. R.K. Willardson and A.C. Beer (Academic Press, New York, 1966) pp. 75–100.
[9] E.O. Kane, in: *Handbook on Semiconductors*, Vol. 1, ed. W. Paul (North-Holland, Amsterdam, 1982) pp. 193–217.
[10] M. Cardona, N.E. Christensen, and G. Fasol, Terms linear in **k** in the band structure of zinc-blende-type semiconductors, Phys. Rev. Lett. **56**(26), 2831–2833 (1986).
[11] M. Cardona, N.E. Christensen, and G. Fasol, Relativistic band structure and spin–orbit splitting of zinc-blende-type semiconductors, Phys. Rev. B **38**(3), 1806–1827 (1988).
[12] B.A. Foreman, Strong linear-**k** valence-band mixing at semiconductor heterojunctions, Phys. Rev. Lett. **86**(12), 2641–2644 (2001).
[13] J.M. Luttinger and W. Kohn, Motion of electrons and holes in perturbed periodic fields, Phys. Rev. **97**(4), 869–883 (1955).
[14] A. Dargys, Luttinger–Kohn Hamiltonian and coherent excitation of the valence-band holes, Phys. Rev. B **66**(16), 165216-1–8 (2002).
[15] I. Vurgaftman, J.R. Meyer, and L.R. Ram-Mohan, Band parameters for III–V compound semiconductors and their alloys, J. Appl. Phys. **89**(11), 5815–5875 (2001).
[16] G. Dresselhaus, Spin–orbit coupling effects in zinc blende structures, Phys. Rev. **100**(2), 580–586 (1955).
[17] L. Reggiani (ed.), *Hot Electron Transport in Semiconductors*, Topics in Applied Physics, Vol. 56 (Springer, Berlin, 1985).
[18] C. Kittel, *Quantum Theory of Solids* (Wiley, New York, 1963) Chapter 9.
[19] G.H. Golub and C.F. Van Loan, *Matrix Computations* (The John Hopkins University Press, Baltimore, 1989) Chapter 8.
[20] W.H. Press, S.A. Teukolsky, W.T. Vetterling, and B.P. Flannery, *Numerical Recipes in Fortran* (Cambridge University Press, Cambridge, 1992) Chapter 2.

SKYLĖS SUKINIO PAVIRŠIAI A_3B_5 PUSLAIDININKIUOSE

A. Dargys

Puslaidininkių fizikos institutas, Vilnius, Lietuva

Santrauka

Puslaidininkių, kurių elementarusis narvelis nepasižymi erdvine inversija, hamiltonianas yra sudarytas iš kvadratinių ir tiesinių pagal bangos skaičių **k** narių. Vyraujantis, kartu ir puslaidininkio savybes lemiantis, dažniausiai yra kvadratinis narys. Todėl, pavyzdžiui, nagrinėjant A_3B_5 puslaidininkių pernašą, tiesinis narys atmetamas. Kol kas nėra aišku, ar skylės sukinio savybes taip pat lemia tik kvadratinė pagal **k** valentinės juostos hamiltoniano dalis. Išnagrinėta kvadratinio ir tiesinio pagal **k** narių įtaka skylės sukinio savybėms GaAs, InAs, GaP, InP, GaSb ir InSb junginiuose. Iš šio darbo matyti, kad išvardintuose A_3B_5 puslaidininkiuose skylės sukinio savybes taip pat lemia aukštesni, t. y. kvadratiniai pagal bangos vektorių, nariai valentinės juostos hamiltoniane. Dėl šios priežasties su sukiniu susietos skylės savybės turėtų būti panašios į elementarių puslaidininkių, kurių elementarioji gardelė pasižymi inversijos simetrija, pavyzdžiui, p tipo silicio, savybes. Grafiškai ir lentelių pavidalu aprašyti sunkiosios bei lengvosios skylės sukinio paviršiai. Taip pat yra pateikti parametrai, kurie leidžia kiekybiškai spręsti apie kvadratinių ir tiesinių narių svarbą (ypač žr. 2 lentelę). Rasta, kad tiesinių narių įtaka sunkiosios masės skylės sukiniui visuose minėtuose junginiuose yra labai maža.